OPEN

Telomere Dysfunction in Renal Tubular Epithelial Cells Leads to Kidney Fibrosis

Sarita Saraswati,[1] *Paula Martínez,*[1] *Rosa Serrano,*[1] *Diego Mejías*[2,3] *Osvaldo Graña-Castro*[4,5] *Ruth Álvarez Díaz*[4] *Juana María Flores*[6] *and Maria A. Blasco*[1]

Key Points

- Trf1 deletion in renal tubular epithelial cells led to renal tubulointerstitial fibrosis, contributing to CKD pathogenesis and progression.
- Loss of Trf1 induced cellular senescence, DNA damage, and telomere shortening and activated regenerative repair.
- Trf1 deletion triggered kirsten rat sarcoma viral oncogene homolog and TNF-α signaling through NF-κB pathway in renal tubules, suggesting a key molecular mechanism in CKD progression.

Abstract

Background Renal tubular epithelial cells are the critical mediators of kidney fibrogenesis. Telomere dysfunction has been associated with kidney injury and fibrosis. However, the role of telomere dysfunction specifically in renal tubular epithelial cells in the onset and progression of kidney fibrosis remains poorly understood. TRF1 is a critical component of the telomeric protective complex known as shelterin, and its deficiency results in telomere dysfunction.

Methods To investigate the impact of telomere dysfunction on kidney injury and fibrosis, we generated mice depleted for the shelterin component TRF1 specifically in renal tubular epithelial cells.

Results Genetic ablation of *Trf1* caused decline in kidney function accompanied by increased tubular injury and tubulointerstitial fibrosis 8 weeks after TRF1 depletion, concomitant with excessive accumulation of extracellular matrix, cell cycle arrest at G2/M phase, and telomeric damage. $Trf1^{\Delta/\Delta}$ mice activated regenerative repair mechanisms, supporting proliferation-mediated telomere shortening in renal tubular epithelial cells. At humane end point, $Trf1^{\Delta/\Delta}$ mice displayed elevated urinary albumin-to-creatinine ratio (UACR), associated with augmented interstitial fibrosis and tubular atrophy eventually leading to CKD. At the mechanistic level, we reported the unprecedented finding that *Trf1* deletion upregulates the Ras–Raf–Mek–Erk, PI3k/Akt/mammalian target of rapamycin, and p38 pathways.

Conclusions Our study underlies a role of renal tubular epithelial cells in the development and progression of kidney fibrosis and CKD induced by telomere dysfunction.

JASN 00: 1–16, 2025. doi: https://doi.org/10.1681/ASN.0000000771

Introduction

CKD is a global public health problem, involving about 10% of the global population, especially in elderly.[1,2] Compared with young individuals, the elderly have higher incidence of CKD-associated morbidity and mortality.[1] Kidney fibrosis is a common pathology in CKD, characterized by increased numbers of myofibroblast, the accumulation extracellular matrix (ECM) in the

[1]Telomeres and Telomerase Group - Fundación Humanismo y Ciencia, Molecular Oncology Program, Spanish National Cancer Centre (CNIO), Madrid, Spain
[2]Confocal Microscopy Unit, Biotechnology Program, Spanish National Cancer Centre (CNIO), Madrid, Spain
[3]Advanced Optical Microscopy Unit, UCCTs, Instituto de Salud Carlos III (ISCIII), Madrid, Spain
[4]Bioinformatics Unit, Structural Biology and Biocomputing Program, Spanish National Cancer Centre (CNIO), Madrid, Spain
[5]Department of Basic Medical Sciences, Institute of Applied Molecular Medicine (IMMA-Nemesio Díez), School of Medicine, San Pablo-CEU University, CEU Universities, Madrid, Spain
[6]Animal Surgery and Medicine Department, Faculty of Veterinary Science, Complutense University of Madrid, Madrid, Spain

Correspondence: Dr. Maria A. Blasco, email: mblasco@cnio.es

Received: January 15, 2025 **Accepted:** July 3, 2025
Published Online Ahead of Print: July 8, 2025

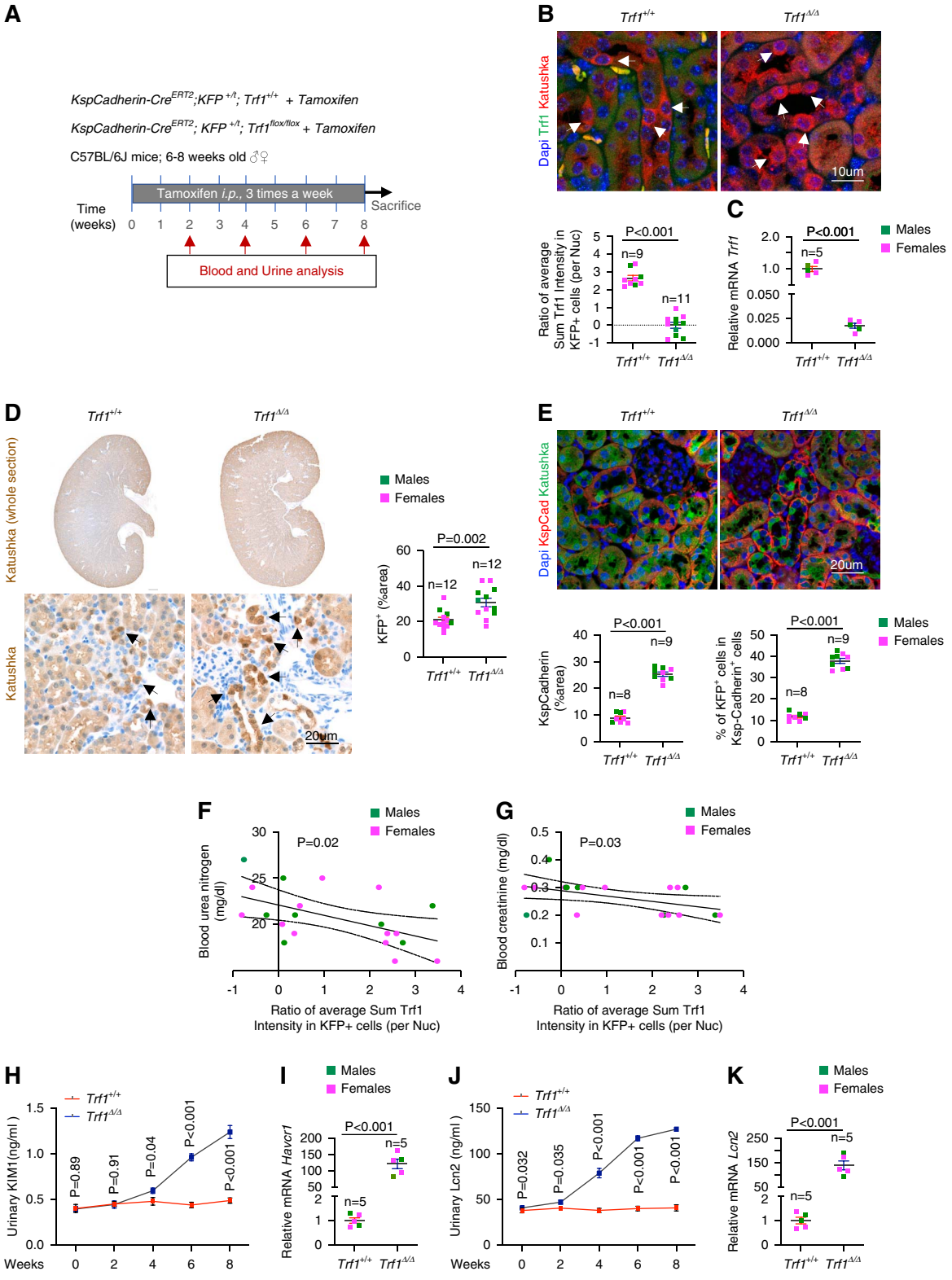

Figure 1. Genetic targeting of *Trf1* in renal tubular epithelial cells was associated with decline in kidney function after injury. (A) Schematic representation of the experimental design. (B) Representative immunofluorescence stainings (6–8 visual fields for each tissue analyzed) for Trf1 (green) and KFP (red) and quantification of ratio of average sum Trf1 intensity in KFP^+ cells (per Nuc) in $Trf1^{+/+}$ and $Trf1^{\Delta/\Delta}$ mice. Nuclei are stained with DAPI (blue). $n=9$ for $Trf1^{+/+}$ (three males, six females) and $n=11$ for $Trf1^{\Delta/\Delta}$ (six males; five females). No statistically significant differences were observed between sexes. (C) Relative mRNA expression of *Trf1* from FACs isolated $EPCAM^+KFP^+$ cells in $Trf1^{+/+}$ and $Trf1^{\Delta/\Delta}$ kidneys. $n=5$ (two males; three females) mice for each group. (D) Representative images (12–15 visual fields for each tissue analyzed) and quantifications of immunostaining of KFP^+ area in whole section of $Trf1^{+/+}$ and

Figure 1. *Continued.* $Trf1^{\Delta/\Delta}$ kidneys (whole section-top panel; magnified view-lower panel). n=12 for $Trf1^{+/+}$ (three males; nine females) and n=12 for $Trf1^{\Delta/\Delta}$ (six males; six females). No statistically significant differences were observed between sexes. (E) Immunofluorescence (6–8 visual fields for each tissue analyzed) of Ksp-Cadherin$^+$ (red) and KFP$^+$ (green) and quantification of the percent Ksp-Cadherin$^+$ and KFP$^+$Ksp-Cadherin$^+$ cells per total number of KFP$^+$ renal tubular epithelial cells of $Trf1^{+/+}$ and $Trf1^{\Delta/\Delta}$ kidneys. n=8 for $Trf1^{+/+}$ (three males; five females) and n=9 for $Trf1^{\Delta/\Delta}$ *mice* (five males; four females). No statistically significant differences were observed between sexes. (F and G) The correlation between ratio of average sum Trf1 intensity in KFP$^+$ cells and kidney function (F) BUN (G) blood creatinine. n=9 for $Trf1^{+/+}$ (three males; six females) and n=11 for $Trf1^{\Delta/\Delta}$ (five males; six females) mice. No statistically significant differences were observed between sexes. (H) ELISA of urinary Kim1. n=6 mice for each group (three males; three females). No statistically significant differences were observed between sexes. (I) Relative mRNA expression of *Kim1* from FACs isolated EPCAM$^+$KFP$^+$ cells in the kidneys of $Trf1^{+/+}$ and $Trf1^{\Delta/\Delta}$ mice. n=5 mice (two males; three females) for each group. (J) ELISA of urinary Lcn2. n=6 mice for each group (three males; three females). No statistically significant differences were observed between sexes. (K) Relative mRNA expression of *Lcn2* from FACs isolated EPCAM$^+$KFP$^+$ cells in the kidneys of $Trf1^{+/+}$ and $Trf1^{\Delta/\Delta}$ mice. n=5 mice (two males; three females) for each group. Male mice are represented in green, and females are represented in pink color. Data are represented as mean±SEM. An unpaired, two-tailed Student t test was used. DAPI, 4′,6-diamidino-2-phenylindole; FACs, fluorescence-activated cell sorting; i.p., intraperitoneally; KFP, Katushka fluorescent protein; Kim-1, kidney injury molecule 1.

tubulointerstitial space, tubular atrophy, microvascular rarefaction, renin-angiotensin-aldosterone system (RAAS) activation, loss of kidney parenchyma, and cellular senescence, ultimately leading to kidney failure.[3] Renal tubular epithelial cells are the most predominant cell type susceptible to various insults, maladaptive or failed regeneration, a hallmark of CKD, known to be the primary source of renal inflammation and fibrogenesis. With aging, injured tubular cells become more sensitized to G2/M arrest inducing a proinflammatory and profibrotic phenotype.[3,4] Renal tubular epithelial cells are also critical in the context of AKI, as they are the primary cell type affected by AKI.[3,4] Given their pivotal role in both adaptive and maladaptive repair after injury, the fate of renal tubular epithelial cells plays a major role in determining the progression or recovery of kidney function.[5] Hallmarks of cellular aging include telomere attrition, cellular senescence (stress-induced premature senescence), DNA damage, mitochondria dysfunction, inflammation, oxidative stress, and epigenetic alterations, among others.[3,4] Injury to kidney cells leads to epithelial-to-mesenchymal transition (EMT) and results in the senescence-associated secretory phenotype and inflammation, eventually leading to the development of fibrosis and CKD.[4,6]

Telomeres are heterochromatic structures at chromosome ends, with tandem repeats of TTAGGG sequence bound by a six-protein complex known as shelterin, encompassing TIN2, TRF1, TRF2, TPP1, POT1, and RAP1, that are essential for chromosome stability and safeguards telomeres by preventing end-to-end chromosome fusions, telomere fragility, and activation of DNA damage response (DDR).[7–9] Telomeres shorten with each cell division and undergo apoptosis and/or cell cycle arrest due telomere uncapping.[10] Telomerase, consists of a catalytic subunit (telomerase reverse transcriptase) and RNA component (Terc), can offset telomere shortening by adding telomeric repeats *de novo*.[7] TRF1 is known to regulate telomere length and capping and prevent replication fork stalling at telomeres.[7,11,12] TRF1 abrogation leads to rapid cellular senescence due to activation of DDR, underscoring the crucial function of TRF1 in averting DNA damage at telomeres.[12,13] *Trf1* deletion has been also shown to be sufficient to induce pulmonary fibrosis[14–16] and bone marrow failure.[17] Telomere dysfunction has been associated to loss of kidney function with increased senescence and apoptosis in response to injury.[18–22] We have previously demonstrated that either telomere shortening associated to telomerase deficiency or telomere dysfunction due to depletion of TRF1 was sufficient to induce interstitial fibrosis in the kidney, recapitulating human disease.[23] Despite considerable progress in understanding the biologic functions of telomeres in kidney function and aging, the cellular origin of telomere dysfunction in the progression of kidney fibrosis remains unknown to date. In a recent work, we showed that deleting *Trf1* specifically in fibroblasts for 8 weeks did not induce kidney fibrosis but triggered inflammatory responses, ECM deposition, cell cycle arrest, fibrogenesis, and vascular rarefaction. Notably, prolonged deletion of *Trf1* in fibroblasts resulted in kidney fibrosis driven by macrophage-to-myofibroblast transition, endothelial-to-mesenchymal transition, and EMT.[24]

In this study, we assessed the role of renal tubular epithelial cells in the origin of kidney fibrosis induced by telomere dysfunction. We explored the effect of TRF1-induced telomere dysfunction in the progression of fibrosis at both short-term deletion (8 weeks since *Trf1* deletion) and long-term deletion (until the humane end point) and using folic acid–induced nephropathy model. We recapitulated the main clinical features observed in patients with CKD in mice lacking TRF1 specifically in renal tubular epithelial cells, including severe telomere shortening over time.

Methods

Mice

$Trf1^{lox/lox}$ mice were generated as previously described.[12] $Trf1^{lox/lox}$ mice were crossed with transgenic mice expressing Cre^{ERT2} under the control of the *KspCadherin-*Cre^{ERT2} promoters as well as with transgenic mice harboring the Katushka fluorescent protein (KFP) encoding gene that contains a stop cassette flanked by lox sequences, the $KFP^{CAG\text{-}lox\text{-}STOP\text{-}lox}$ allele[25–27] (Supplemental Figure 1A). Tamoxifen (TMX)–inducible *KspCadherin-*Cre^{ERT2} frozen sperms were kindly provided by Prof. Dorien J.M Peters, Department of Human Genetics at the Leiden University Medical Center. TMX was intraperitoneally injected to 6- to 8-week-old male and female $Trf1^{+/+}$ and $Trf1^{lox/lox}$ mice.

Folic Acid Nephropathy Mouse Model

Single intraperitoneal injection of folic acid with a low dose of 125 mg kg/body weight dissolved in vehicle

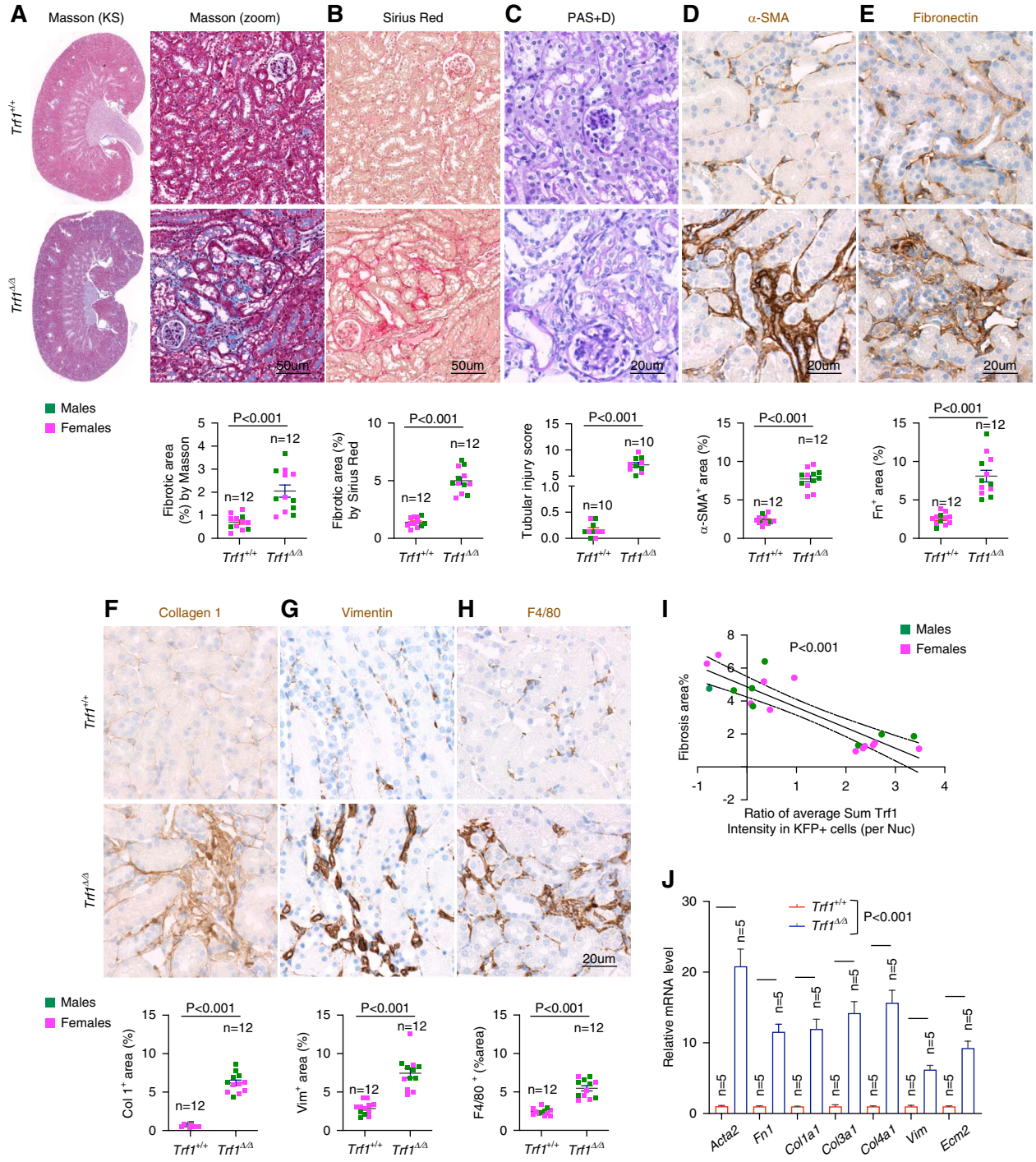

Figure 2. Renal tubular epithelial cell–specific Trf1 deletion led tubulointerstitial fibrosis and tubular damage. (A–C) Representative images of staining and quantifications (whole section analyzed). (A) Masson trichome staining in whole section of $Trf1^{+/+}$ and $Trf1^{\Delta/\Delta}$ kidneys (whole section-left panel; magnified view-right panel). n=12 for $Trf1^{+/+}$ (three males; nine females) and n=12 for $Trf1^{\Delta/\Delta}$ (six males; six females) mice. No statistically significant differences were observed between sexes. (B) Sirius red staining in $Trf1^{+/+}$ and $Trf1^{\Delta/\Delta}$ kidneys. n=12 for $Trf1^{+/+}$ (three males; nine females) and n=12 for $Trf1^{\Delta/\Delta}$ (six males; six females) mice. No statistically significant differences were observed between sexes. (C) PAS+D staining (12–15 visual fields for each tissue analyzed) and quantifications of tubular injury score. n=10 mice for each group (five males; five females). No statistically significant differences were observed between sexes. (D–H) Representative images of immunostaining and quantifications (whole section analyzed; D) α-SMA, (E) fibronectin (Fn^+), (F) collagen 1 (Col 1^+), (G) vimentin (Vim^+), and (H) F4/80 in t $Trf1^{+/+}$ and $Trf1^{\Delta/\Delta}$ kidneys. n=12 for $Trf1^{+/+}$ (three males; nine females) and n=12 for $Trf1^{\Delta/\Delta}$ (six males; six females) mice. No statistically significant differences were observed between sexes. (I) The correlation between ratio of average sum Trf1 intensity in KFP^+ cells and kidney fibrosis. n=9 for $Trf1^{+/+}$ (three

Figure 2. *Continued.* males; six females) and n=11 for $Trf1^{\Delta/\Delta}$ (five males; six females) mice. No statistically significant differences were observed between sexes. (J) Relative mRNA expression of *Acta, Fn, Col1a1, Col3a1, Col4a1, Vim, Ecm2* in $Trf1^{+/+}$ and $Trf1^{\Delta/\Delta}$ kidneys. n=5 mice (two males; three females) for each group. Male mice are represented in green, and females are represented in pink color. Data are represented as mean±SEM. An unpaired, two-tailed Student t test was used. α-SMA, alpha-smooth muscle actin; PAS+D, periodic acid–Schiff with diastase.

(200 μl of 0.3 M $NaHCO_3$) or vehicle alone (200 μl of 0.3 M $NaHCO_3$) was administered to $Trf1^{+/+}$ and $Trf1^{\Delta/\Delta}$ mice after a 4-week period of administration.

Telomere Quantitative Fluorescence *In Situ* Hybridization Analyses

Telomere quantitative-FISH was performed on paraffin-embedded tissue sections as previously described.[16,23]

Detailed methods involved in the manuscript are listed in Supplemental Methods and Supplemental Table 2.

Statistics

Mice were randomly assigned to groups, and investigators were blinded to group allocation. Sample sizes corresponded to the number of mice used for each experiment, as indicated. For single immunohistochemistry (IHC) stainings, whole kidney sections were quantified. For double IHC stainings, quantification was performed in whole kidney section comprising 12–15 areas. For immunofluorescence analysis, 6–8 images were collected from each individual. Data distribution was assumed to be normal, but this was not formally tested. No data points or mice were excluded, and the results were presented as the mean±SEM. An unpaired, two-tailed Student t test was used for comparison between groups. Statistical analysis was performed using GraphPad Prism version 9 (version 9.5.1-528) software. The significance was set at a P value of < 0.05. Overall survival was assessed by the Kaplan–Meier survival curves using the log rank (Mantel–Cox) test.

Results

Trf1 Deletion in Renal Tubular Epithelial Cell Induced Tubulointerstitial Fibrosis, Functional Decline, and Persistent Tubular Injury

To induce both *Trf1* deletion and KFP expression, TMX was administered intraperitoneally in 6- to 8-week-old male and female mice three times per week for 8 consecutive weeks (Figure 1A). Immunofluorescence staining confirmed the absence of TRF1 fluorescent signals in KFP^+ renal tubular epithelial cells of $Trf1^{\Delta/\Delta}$ mice, in contrast to detection of TRF1 signals in $Trf1^{+/+}$ mice, confirming that $Trf1^{\Delta/\Delta}$ mice underwent successful Ksp-Cre–mediated recombination and *Trf1* deletion (Figure 1B). We confirmed these findings by reverse transcription quantitative PCR (RT-qPCR) of *Trf1* mRNA levels, which was found to be downregulated in $Trf1^{\Delta/\Delta}$ mice compared with $Trf1^{+/+}$ mice in fluorescence-activated cell sorting sorted $EPCAM^+KFP^+$ renal tubular epithelial cells (Figure 1C). Immunohistochemistry analysis demonstrated two-fold increase in both KFP^+ and $KspCad^+$ expression and three-fold increase in $KFP^+KspCad^+$ cells in $Trf1^{\Delta/\Delta}$ mice compared with $Trf1^{+/+}$ mice (Figure 1, D and E). *Trf1* deletion was significantly positively correlated with plasma creatinine levels and BUN levels (Figure 1, F and G). Plasma creatinine and BUN levels showed sustained elevation in $Trf1^{\Delta/\Delta}$ mice compared with $Trf1^{+/+}$ mice after 6 weeks of *Trf1* deletion (Supplemental Figure 1, B and C). Physiologic evaluation indicated no significant differences in liver function, glucose metabolism, and other kidney functions between $Trf1^{\Delta/\Delta}$ and $Trf1^{+/+}$ mice (Supplemental Figure 1, D–M). No alterations in body weight or kidney-to-body weight ratio were observed (Supplemental Figure 1, N and O). $Trf1^{\Delta/\Delta}$ mice exhibited a progressive rise in urinary kidney injury molecule 1 (Kim-1) and lipocalin-2 (Lcn2) levels, as early as 4 weeks post-*Trf1* ablation (Figure 1, H and J). Simultaneously, *Kim-1* (*Havcr1*) and *Lcn2* mRNA expression was also significantly higher in $Trf1^{\Delta/\Delta}$ kidneys (Figure 1, I and K). Masson and Sirius red staining displayed marked increase in collagen deposition along with loss of basement membrane and tubular atrophy in $Trf1^{\Delta/\Delta}$ (Figure 2, A–C). TRF1 abrogation significantly upregulated alpha-smooth muscle actin (α-SMA), fibronectin, collagen 1, vimentin, and F4/80 expression leading to increased fibrosis in $Trf1^{\Delta/\Delta}$ kidneys as compared with $Trf1^{+/+}$ mice (Figure 2, D–I). RT-qPCR further confirmed the upregulation of *Acta2*, *Fn1*, *Col1a1*, *Col3a1*, *Col4a1*, *Vim*, and *Ecm2* mRNA levels in $Trf1^{\Delta/\Delta}$ kidneys (Figure 2J). Increased expression of keratins KRT-7, KRT-8, KRT-18, and KRT-19 by injured tubules has been reported in both human and experimental models of kidney disease.[28] No prior sample size calculation was made. $Trf1^{\Delta/\Delta}$ mice displayed five-fold increase in $Krt8/18^+KFP^+$-positive cells in the renal tubules (Supplemental Figure 1P). Histopathologic analysis, after 8 weeks of TMX administration, of other organs (heart, liver, and lung) examined by hematoxylin and eosin and Masson staining revealed no histologic abnormalities (Supplemental Figure 2). These results indicate that TRF1 depletion in renal epithelium leads to kidney fibrogenesis.

Trf1 Deletion in Renal Tubular Epithelial Cells Induced Cellular Senescence, DNA Damage, and G2/M Arrest

To address the molecular effects of *Trf1* deletion in renal tubular epithelial cells, we analyzed the expression of senescence markers p53/p21 and senescence-associated secretory phenotype as well as determined the DNA damage burden in fluorescence-activated cell sorting sorted $EPCAM^+KFP^+$ renal tubular epithelial cells. IHC staining with p21 and p53 demonstrated an eight-fold and four-fold increase in *Trf1*-deleted $p21^+KFP^+$ and $p53^+KFP^+$ cells, respectively, as compared with $Trf1^{+/+}$ mice (Figure 3, A and B). Similarly, senescence-associated β-galactosidase–positive cells were readily detectable in $Trf1^{\Delta/\Delta}$ kidneys and almost absent in $Trf1^{+/+}$ kidneys (Figure 3C). $Trf1^{\Delta/\Delta}$ mice had significant decrease in telomere intensity in renal tubular epithelial cells compared with $Trf1^{+/+}$ mice (Figure 3D), suggesting that telomere shortening might arise as a

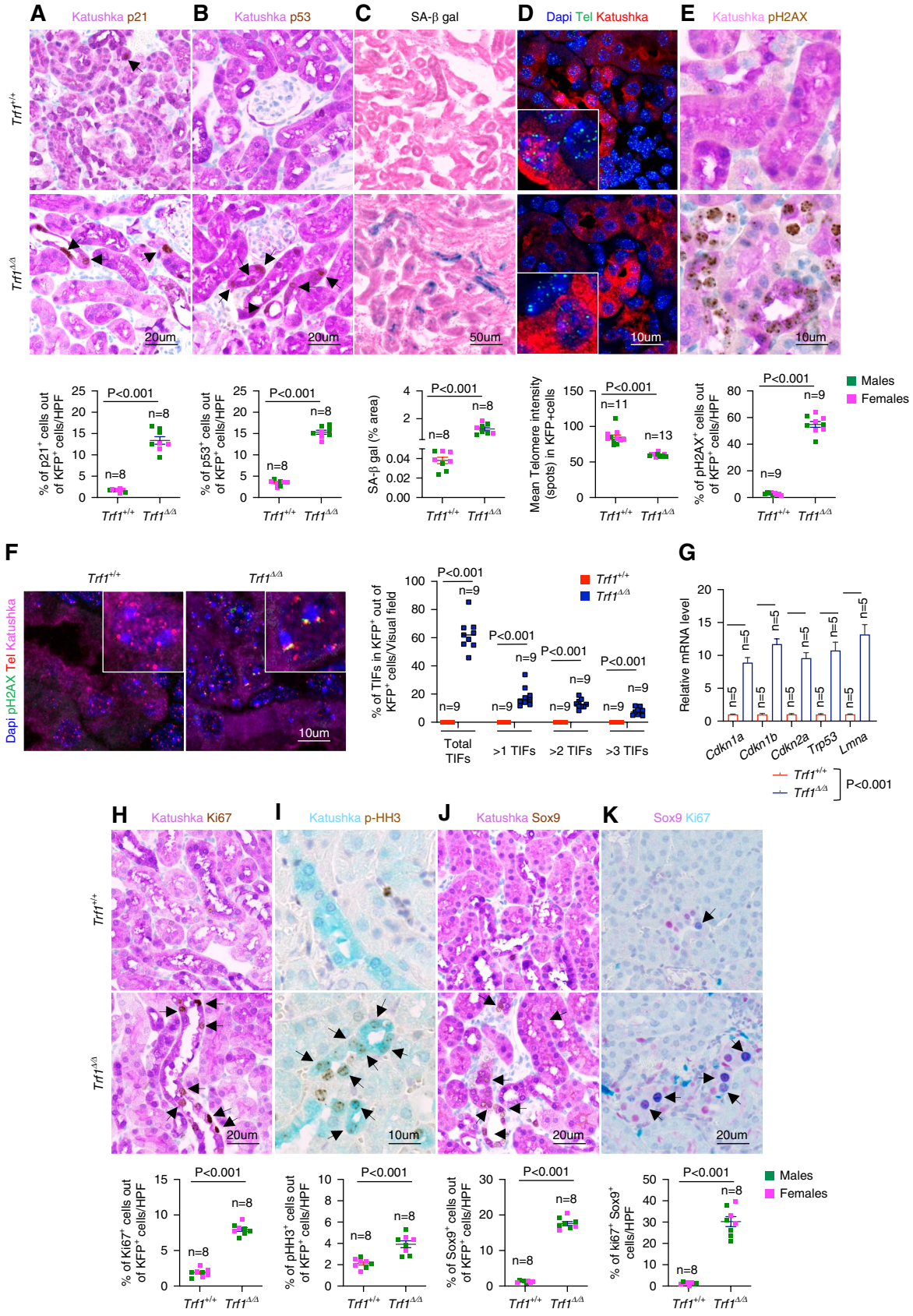

Figure 3. *Trf1* deletion in renal tubular epithelial cells led to cell cycle arrest and telomeric damage and prompted regenerative repair. (A–E) Representative images (12–15 visual fields for each tissue analyzed) and quantifications of multiplex staining per total number of KFP$^+$ renal tubular epithelial cells of *Trf1*$^{+/+}$ and *Trf1*$^{\Delta/\Delta}$ kidneys of (A) KFP$^+$p21$^+$ cells and (B) KFP$^+$p53$^+$cells. n=8 for

Figure 3. *Continued.* $Trf1^{+/+}$ (three males; five females) and $n=8$ for $Trf1^{\Delta/\Delta}$ (five males; three females) mice. No statistically significant differences were observed between sexes. (C) Representative images and quantifications (whole section analyzed) of SA-β-gal staining in $Trf1^{+/+}$ and $Trf1^{\Delta/\Delta}$ kidneys. $n=8$ for $Trf1^{+/+}$ (four males; four females) and $n=8$ for $Trf1^{\Delta/\Delta}$ (five males; three females) mice. No statistically significant differences were observed between sexes. (D) Representative images (6–8 visual fields for each tissue analyzed) of immuno-telomere QFISH in KFP^+ renal tubular epithelial cells (Cy3Tel probe (green), KFP^+ cells (red) and quantification of mean telomere spot intensity in $Trf1^{+/+}$ and $Trf1^{\Delta/\Delta}$ kidneys. Nuclei are stained with DAPI (blue). $n=11$ for $Trf1^{+/+}$ (five males; six females) and $n=13$ for $Trf1^{\Delta/\Delta}$ (8 males; five females) mice. No statistically significant differences were observed between sexes. (E) Representative images (12–15 visual fields for each tissue analyzed) and quantifications of multiplex staining of KFP^+pH2AX^+ cells per total number of KFP^+ renal tubular epithelial cells of $Trf1^{+/+}$ and $Trf1^{\Delta/\Delta}$ kidneys. $n=9$ for $Trf1^{+/+}$ (five males; four females) and $n=9$ for $Trf1^{\Delta/\Delta}$ (four males; five females) mice. No statistically significant differences were observed between sexes. (F) Representative images (6–8 visual fields for each tissue analyzed) of TIFs in KFP^+ renal tubular epithelial cells (magenta), pH2AX (green), telomere (red) and quantification of TIFs in KFP^+ cells in $Trf1^{+/+}$ and $Trf1^{\Delta/\Delta}$ kidneys. Nuclei are stained with DAPI (blue). $n=9$ mice for each group. $n=9$ for $Trf1^{+/+}$ (five males; four females) and $n=9$ for $Trf1^{\Delta/\Delta}$ (four males; five females) mice. No statistically significant differences were observed between sexes. (G) Relative mRNA expression of *Cdkn1a*, *Cdkn1b*, *Cdkn2a*, *Trp53*, and *Lmna* from FACs isolated $EPCAM^+KFP^+$ cells in the kidneys of $Trf1^{+/+}$ and $Trf1^{\Delta/\Delta}$ mice. $n=5$ (two males; three females) mice for each group. (H–K) Representative images of (12–15 visual fields for each tissue analyzed) and quantifications of multiplex staining per total number of KFP^+ renal tubular epithelial cells in $Trf1^{+/+}$ and $Trf1^{\Delta/\Delta}$ kidneys (H) KFP^+Ki67^+ cells, (I) KFP^+pHH3^+, (J) KFP^+Sox9^+ cells, and (K) $Sox9^+Ki67^+$cells. $n=8$ for $Trf1^{+/+}$ (three males; five females) and $n=8$ for $Trf1^{\Delta/\Delta}$ (five males; three females) mice. No statistically significant differences were observed between sexes. Male mice are represented in green, and females are represented in pink color. Data are represented as mean±SEM. An unpaired, two-tailed Student *t* test was used. pH2AX, phosphorylated form of the histone protein H2AX; QFISH, quantitative fluorescence *in situ* hybridization; SA-β-gal, senescence-associated β-galactosidase; TIF, telomere-induced foci.

consequence of increased cell turnover to repair TRF1-induced DNA damage as indicated by elevated number of $KFP^+KspCad^+$ cells (Figure 1, D and E). Analysis of total DNA damage burden as well as telomere-associated DNA damage in renal tubular epithelial cells showed an increase in phosphorylated form of the histone protein H2AX-positive cells in $Trf1^{\Delta/\Delta}$ (Figure 3E). In addition, telomere dysfunction–induced foci were significantly increased in $Trf1^{\Delta/\Delta}$ renal tubular epithelial cells compared with $Trf1^{+/+}$ (Figure 3F). RT-qPCR confirmed the upregulation of *Cdkn1a*, *Cdkn1b*, *Cdkn2a*, *Trp53*, and *Lmna* mRNA levels in $Trf1^{\Delta/\Delta}$ kidneys (Figure 3G). Notably, *Trf1* deletion increased the percentage of KFP^+ cells arrested in the G2 phase based on the higher levels of phospho-histoneH3 at serine10 positive cells showing a foci staining pattern ($p\text{-}H3^+KFP^+$). We observed higher levels of Ki67-positive cells ($Ki67^+KFP^+$) indicating cells proliferation, likely due to an attempt to regenerate, in agreement with higher percentage of $KspCad^+$ cells observed in *Trf1*-depleted kidneys (Figure 1D).

Trf1 Deletion in Renal Tubular Epithelial Cells Activated Regenerative Repair in Injured Kidneys of $Trf1^{\Delta/\Delta}$ Mice

In stress conditions, surviving injured cells switch on Sox9 gene as a response to kidney damage, causing the activation of regeneration and repair mechanism in injured tubules.[29] $Trf1^{\Delta/\Delta}$ mice showed 13-fold upregulation of $Sox9^+KFP^+$ cells in renal tubular epithelial cells, implicating Sox9-mediated transcriptional regulation in early response to tubular injury (Figure 3J). Tubules exhibiting a reparative signature showed higher levels of $Ki67^+$ proliferative cells predominantly within $Sox9^+$ cell fraction of proximal tubule.[29] Concurrently, we showed that a large fraction (30%) of $Sox9^+$ cells were actively proliferating in $Trf1^{\Delta/\Delta}$ mice as compared with $Trf1^{+/+}$ mice (Figure 3K). Our observation further supports proliferation-mediated telomere shortening in tubular cells with increased telomere damage owing to TRF1 abrogation (Figure 3D).

In parallel to interstitial fibrosis, endothelial dysfunction is linked to structural defects of microcirculation, including microvascular rarefaction that may exacerbate renal hypoxia.[30] $Trf1^{\Delta/\Delta}$ mice showed three-fold increase in hypoxia with 35% reduction in vessel density as indicated by elevated numbers of $HIF1a^+KFP^+$ cells and decreased $CD31^+$ area in $Trf1^{\Delta/\Delta}$ kidneys, respectively (Supplemental Figure 3).

Trf1 Deletion in Renal Tubular Epithelial Cells Affected Their Transcriptional Landscape

Gene set enrichment analysis (GSEA) revealed that *Trf1*-deleted renal tubular epithelial cells showed the number of deregulated pathways, including ECM organization (false discovery rate [FDR]=0.09) and receptor interactions (FDR=0.008; Supplemental Figure 4, C and D). IL6-JAK-STAT3 and Tgf-β signaling also showed a trend toward enrichment in IL6-JAK-STAT3–associated genes ($P = 0.164$) and Tgf-β–associated genes ($P = 0.601$) (Supplemental Figure 4, E and F), although they were NS. $Trf1^{\Delta/\Delta}$ mice displayed upregulation of IL6 levels (Supplemental Figure 4G). Immunolabeling of $KFP^+pSTAT3^+$ showed an increase in $Trf1^{\Delta/\Delta}$ compared with $Trf1^{+/+}$ kidneys, suggesting that increased inflammation leads to the activation of IL6-JAK-STAT3 pathway as a consequence of *Trf1*-abrogation (Supplemental Figure 4H). Differentially expressed gene analysis between $Trf1^{\Delta/\Delta}$ and $Trf1^{+/+}$ kidneys revealed a total of 739 genes differentially deregulated (FDR <0.05) between both groups, of which 311 and 428 genes were upregulated and downregulated, respectively, in $Trf1^{\Delta/\Delta}$ *cells*. We generated a heatmap of relative expression of relevant genes and a volcano plot of differentially expressed genes between $Trf1^{\Delta/\Delta}$ and $Trf1^{+/+}$ kidneys, highlighting those genes related to telomere maintenance and repair, fibrosis, kidney damage, inflammation, and mitogen-activated protein kinase (MAPK) gene sets[31] (Figure 4, A and B). The complete lists of deregulated genes are presented in Supplemental Table 1. The expression of telomere maintenance and repair genes was negatively correlated with the expression of genes related to fibrosis and kidney damage as well as with inflammation and MAPK in $Trf1^{\Delta/\Delta}$ mice compared with $Trf1^{+/+}$ mice, suggesting that telomere

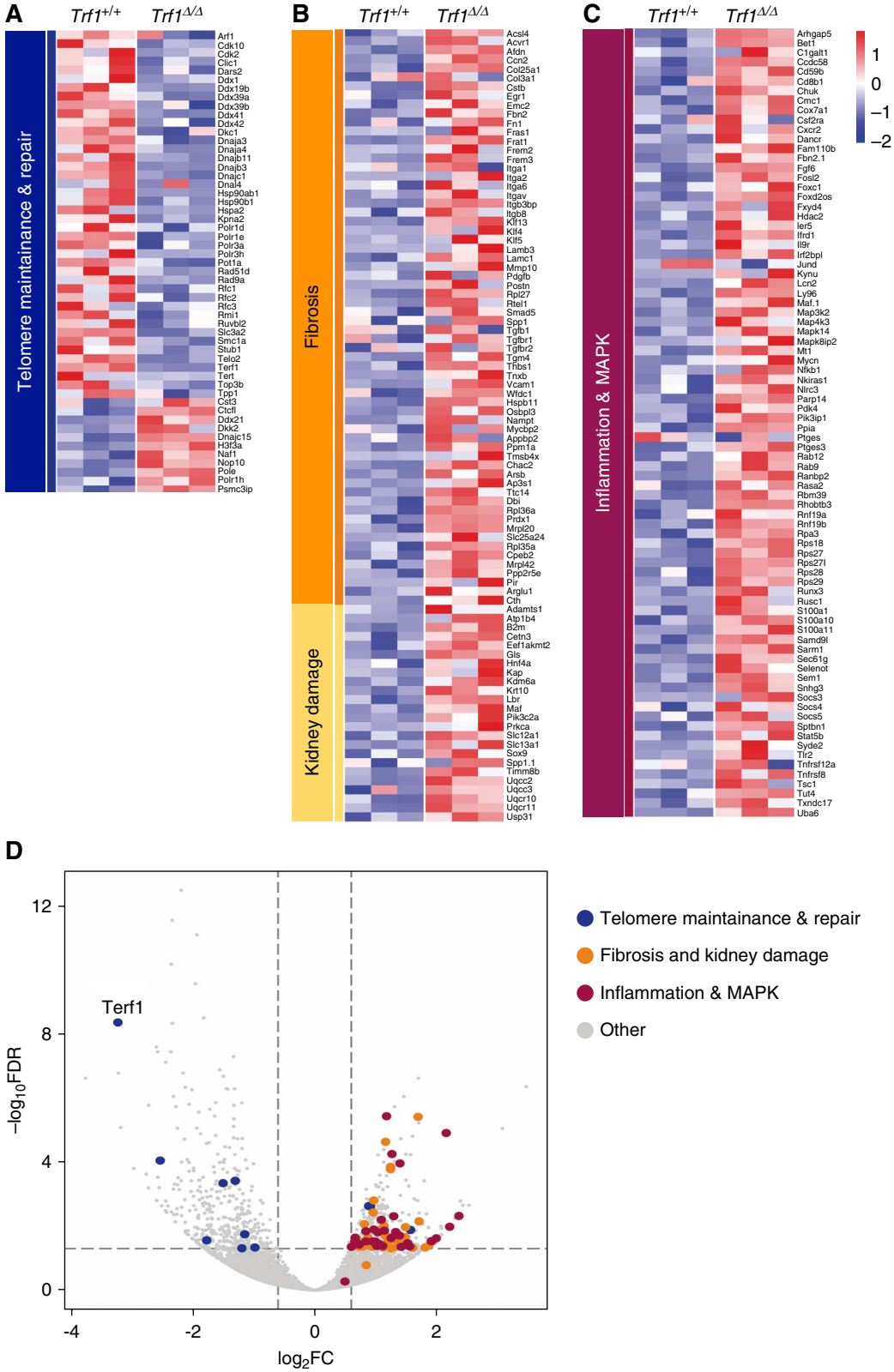

Figure 4. Transcriptome analysis by RNA-seq showing the DEGs. The heatmap of the DEGs of (A) telomere maintenance and repair, (B) fibrosis and kidney damage, and (C) inflammation and MAPK among $Trf1^{+/+}$ and $Trf1^{\Delta/\Delta}$ mice. (D) Volcano plot showing all the gene expression pattern of up- or downregulated DEGs in $Trf1^{+/+}$ and $Trf1^{\Delta/\Delta}$ mice. The *x*-axis depicts the $\log_2$ fold change in gene expression. The *y*-axis depicts the $-\log_{10}$ FDR value. The blue color represents downregulated genes of telomere maintenance and repair, and orange and red color represents upregulated genes of fibrosis, kidney damage inflammation and MAPK, respectively. DEG, differentially expressed gene; FC, fold change; FDR, false discovery rate; Lcn2, lipocalin-2; MAPK, mitogen-activated protein kinase.

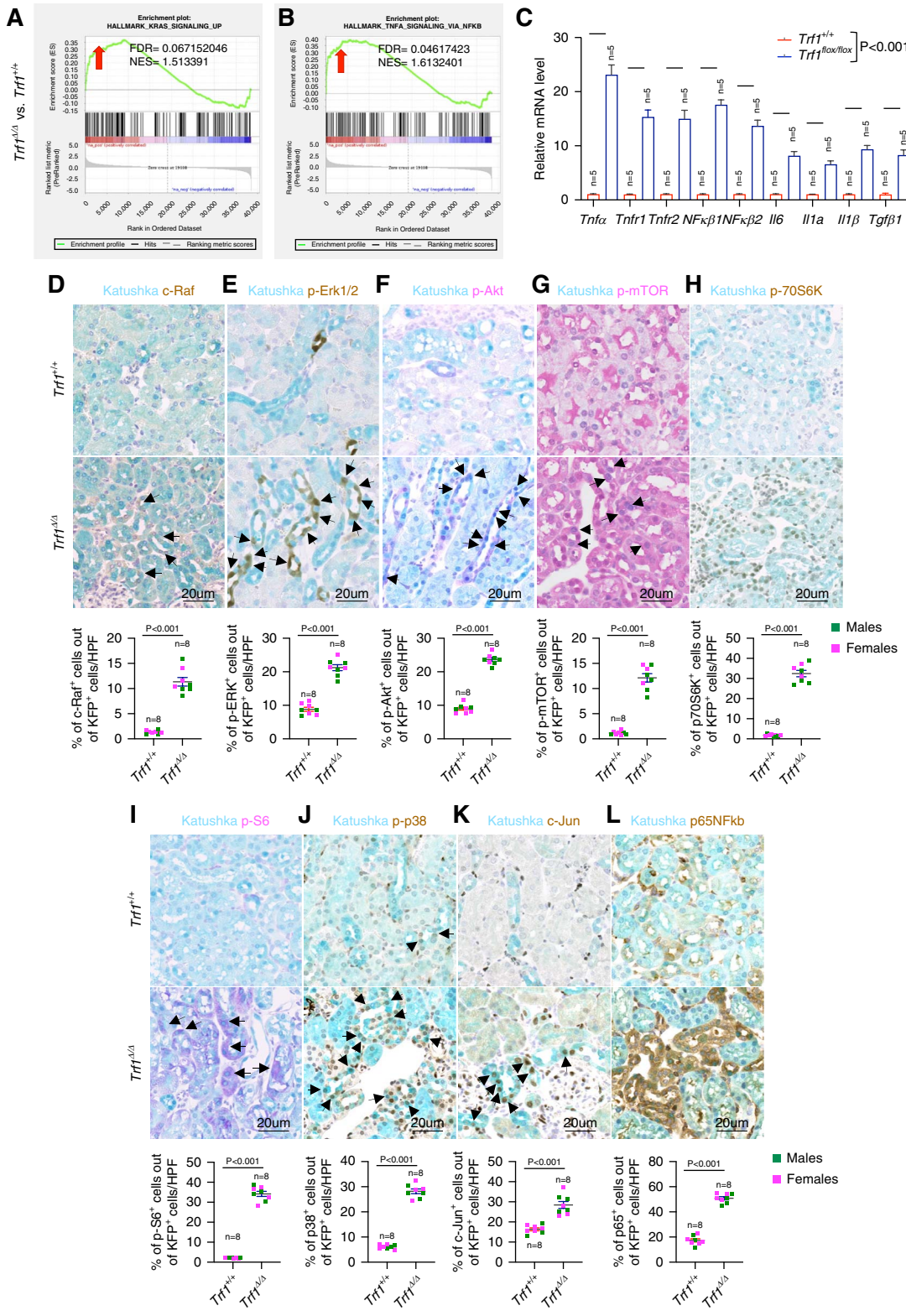

Figure 5. *Trf1* deletion in renal tubular epithelial cells activated KRAS signaling and TNF-α signaling through NFκB pathway. GSEA enrichment plots of hallmark gene dataset showing enriched pathways (FDR <25%). (A) KRAS signaling up. (B) Tnf-α signaling through NFκb in the kidneys of $Trf1^{+/+}$ and $Trf1^{\Delta/\Delta}$ mice. n=3 mice for each group. (C) Relative mRNA expression of *Tnfa*, *Tnfr1*, *Tnfr2*, *NFκβ1*, *NFκb2*, *Il6*, *Ila1*, *Il1b*, *Tgfβ1*, and *Ccl2* in $Trf1^{+/+}$ and $Trf1^{\Delta/\Delta}$ kidneys. n=5 mice (two males; three females) for each group. (D–H) Representative images of (12–15 visual fields for each tissue analyzed) and quantifications of multiplex staining per total number of KFP^+ renal tubular epithelial cells in $Trf1^{+/+}$ and $Trf1^{\Delta/\Delta}$ kidneys. (D) KFP^+c-Raf^+ cells. (E) KFP^+p-$ERK1/2^+$ cells. (F) KFP^+p-Akt^+ cells. (G) KFP^+p-$mTOR^+$ cells. (H) KFP^+p-$70S6K^+$ cells. n=8 for $Trf1^{+/+}$ (three males; five females) and n=8 for $Trf1^{\Delta/\Delta}$ (five males;

Figure 5. *Continued.* three females) mice. No statistically significant differences were observed between sexes. (I–L) Representative images of (12–15 visual fields for each tissue analyzed) and quantifications of multiplex staining per total number of KFP^+ renal tubular epithelial cells in $Trf1^{+/+}$ and $Trf1^{\Delta/\Delta}$ kidneys. (I) KFP^+p-S6$^+$ cells. (J) KFP^+p-p38$^+$ cells. (K) KFP^+c-Jun$^+$ cells. (L) KFP^+p-p65 NFkb$^+$ cells. n=8 for $Trf1^{+/+}$ (three males; five females) and n=8 for $Trf1^{\Delta/\Delta}$ (four males; four females) mice. No statistically significant differences were observed between sexes. Male mice are represented in green, and females are represented in pink color. Data are represented as mean±SEM. An unpaired, two-tailed Student's t test was used. AKT, protein kinase B; ERK, extracellular signal–regulated kinase; GSEA, gene set enrichment analysis; KRAS, kirsten rat sarcoma viral oncogene homolog; mTOR, mammalian target of rapamycin; NES, normalized enrichment score.

dysfunction in renal tubular epithelial cells drives gene expression programs associated with kidney fibrosis.

Trf1 Deletion Triggered Both Kirsten Rat Sarcoma Viral Oncogene Homolog and TNF-α Signaling through NFκB Pathway in Renal Tubules

GSEA analysis revealed significant enrichment for both kirsten rat sarcoma viral oncogene homolog (KRAS) (normalized enrichment score [NES]: 1.513) and TNF-α signaling through NFκB pathway (NES: 1.613; Figure 5, A and B). RT-qPCR analysis confirmed significant transcriptional upregulation of inflammatory cytokines: *Tnfr1* (*Tnfrsf1a*) and *Tnfr2* (*Tnfrsf1b*), *NF$\kappa\beta$1*, *NF$\kappa\beta$2*, *IL6*, *Il1α*, *IL1β*, *Tgfβ1*, and *CCl2* in the kidneys of $Trf1^{\Delta/\Delta}$ compared with $Trf1^{+/+}$ mice (Figure. 5C). The activation of KRAS is known to initiate several downstream signaling pathways, such as phosphatidylinositol 3-kinase (PI3K)/protein kinase B (AKT) mammalian target of rapamycin (mTOR), MAPK, and NF-κB.[32] Consequently, we determined levels of c-Raf and phosphorylated, p-Erk, p-Akt, p-mTOR, p70S6K, pS6, p38, and c-Jun. Our findings showed significant increase in the percentage of KFP^+c-Raf$^+$, KFP^+pERK^+, KFP^+pAKT^+, $KFP^+p\text{-}mTOR^+$, $KFP^+p70S6K^+$, KFP^+pS6^+, $KFP^+p\text{-}p38^+$, and $KFP^+c\text{-}Jun^+$ double-positive cells in $Trf1^{\Delta/\Delta}$ compared with $Trf1^{+/+}$ mice (Figure 5, D–K). Aberrant NF-κB activation is conventionally defined by increased NF-kappa-B expression.[33] Immunolabeling revealed three-fold increase in coexpressing KFP^+NF-$\kappa\beta$ p65$^+$ cells in renal tubular epithelial cells of $Trf1^{\Delta/\Delta}$ (Figure 5L). We observed preferential staining of pERK, pAKT, cJun, and NF-$\kappa\beta$ p65$^+$ in distal nephron segments with little staining in proximal tubules. By contrast, Raf, S6, p-p38, and p70SK6 staining is clearly more heterogeneous in both proximal and distal segments. In addition, ELISA revealed upregulation of TNF-α levels in $Trf1^{\Delta/\Delta}$ mice (Supplemental Figure 4I). These data support the unprecedented finding that *Trf1* deletion exerts fibrotic activity partially by upregulating the RAS–RAF–mitogen-activated protein kinase (MEK)–extracellular signal[en]regulated kinase (ERK), PI3k/Akt/mTOR, and p38 pathways.

Trf1 Deletion Activated RAAS Pathway in Renal Tubules

Since the activation of RAAS plays a central role in the progression of CKD and congestive heart failure,[34] we analyzed the expression of RAAS components in kidneys. Immunolabeling showed higher angiotensinogen (Agt) and angiotensin-converting enzyme (Ace) expression along the apical border of proximal tubules with four-fold and five-fold increase in Agt$^+$ and Ace$^+$ cells, respectively, in $Trf1^{\Delta/\Delta}$ mice (Supplemental Figure 5, A and B). Angiotensin-converting enzyme 2 (Ace2) deficiency enhances kidney inflammation and kidney fibrosis and exacerbates the progression of CKD.[35] Concurrently, Ace2 expression was lower in $Trf1^{\Delta/\Delta}$ mice compared with $Trf1^{+/+}$ mice (Supplemental Figure 5C). These findings were validated by RT-qPCR, showing upregulation of mRNA levels of *Agt*, *Ren1*, *Ace* and downregulation of *Ace2* in $Trf1^{\Delta/\Delta}$ kidneys compared with $Trf1^{+/+}$ kidneys (Supplemental Figure 5D). Urinary AGT (uAGT) excretion is often used as an indicator of intrarenal RAAS activity.[36] $Trf1^{\Delta/\Delta}$ mice displayed increased urinary AGT levels (Supplemental Figure 5E).

Long-Term *Trf1* Deletion Exacerbated Kidney Fibrosis Leading to CKD

Furthermore, we explored long-term outcomes of targeted renal tubular epithelial injury induced by *Trf1* deletion (Figure 6A). No prior sample size calculation was made. $Trf1^{\Delta/\Delta}$ mice displayed significant reduction in body weight after 8 months of continuous TRF1 depletion, which continued until humane end point, with significant increase in kidney-to-body weight ratio at humane end point in $Trf1^{\Delta/\Delta}$ mice (Supplemental Figure 6, A and B). $Trf1^{\Delta/\Delta}$ mice showed reduced hair density, hair loss (alopecia), and kyphosis (Figure 6B). $Trf1^{\Delta/\Delta}$ kidneys appeared pale and damaged in comparison with $Trf1^{+/+}$ mice (Figure 6C). $Trf1^{\Delta/\Delta}$ mice revealed significantly increased blood creatinine and BUN after 2 months of TMX (Figure 6D and Supplemental Figure 6C). In addition, urinary albumin-to-creatinine ratio (UACR), an early marker of abnormal kidney dysfunction, was significantly higher in $Trf1^{\Delta/\Delta}$ mice compared with $Trf1^{+/+}$ mice after 4 months of TMX (Figure 6E). To further investigate whether the potential effect of observed comorbidities could lead to lower survival, we monitored the mortality rates in mice. Interestingly, despite half of $Trf1^{\Delta/\Delta}$ mice succumbing at early time points, we observed no difference in overall survival between $Trf1^{\Delta/\Delta}$ and $Trf1^{+/+}$ mice (Figure 6F). Survival analysis based on mouse gender revealed no significant longevity differences between both genotypes (Supplemental Figure 6, D and E). Histopathologic examination of all organs indicated that pulmonary pathologies were the primary cause of deterioration and death in both genotypes, with kidney pathologies being more prevalent in $Trf1^{\Delta/\Delta}$ mice (Figure 6G and Supplemental Figure 7A). It is possible that the TMX induced damage to the alveolar walls, resulting in hemorrhages and a large number of hemosiderophages, followed by multifocal hepatitis in the liver (Figure 6G and Supplemental Figure 7, A and B). By contrast, $Trf1^{\Delta/\Delta}$ mice showed 100% incidence of kidney fibrosis and tubular atrophy and degeneration, while none of the $Trf1^{+/+}$ mice presented kidney fibrosis (Figure 6G). Analysis of the heart revealed perivascular and interstitial fibrosis, with

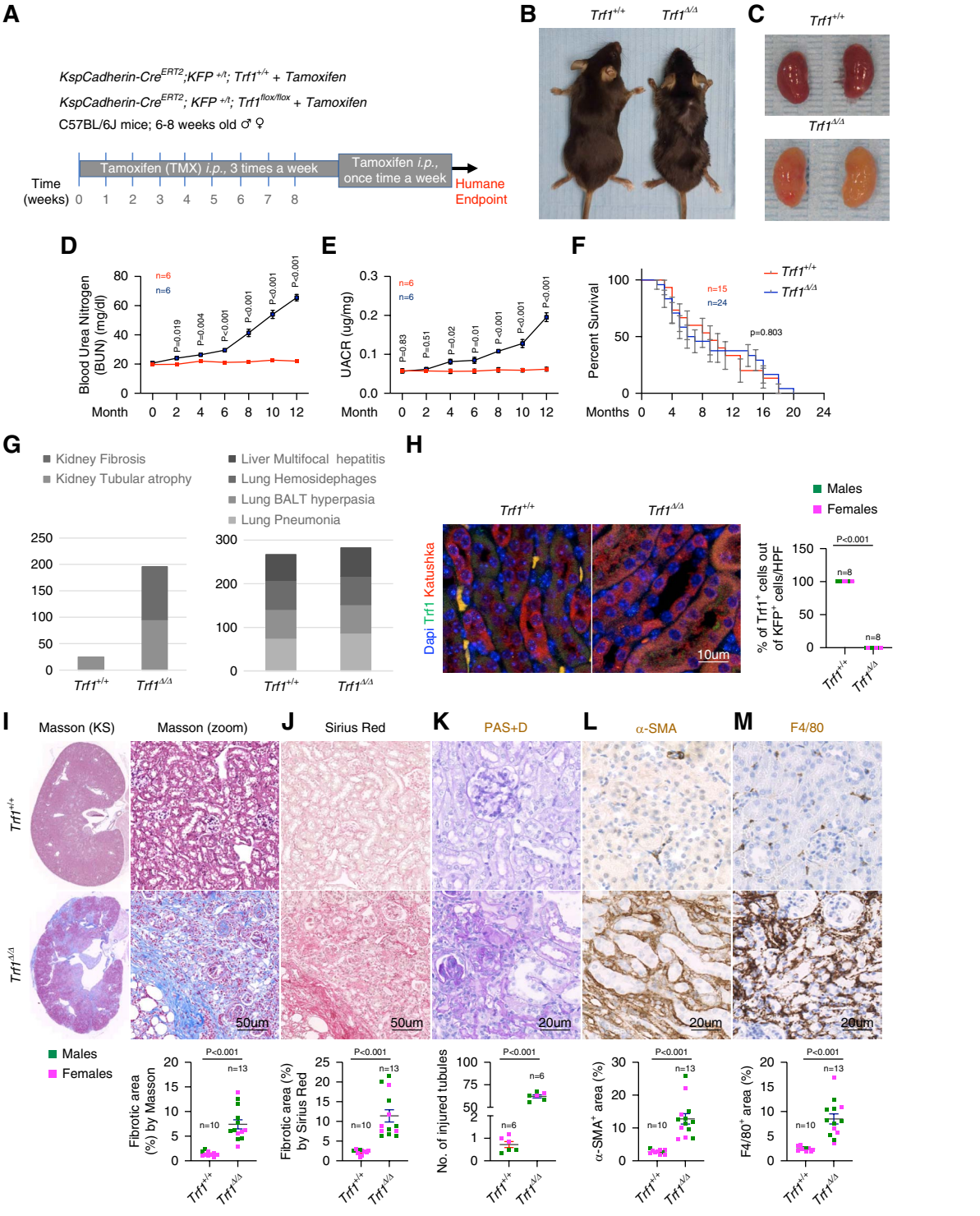

Figure 6. Prolonged renal tubular epithelial cells *Trf1* deletion aggravated kidney fibrosis, contributing to CKD. (A) Schematic representation of the experimental design. (B) Representative images of mice of the indicated genotypes. (C) Macroscopic appearance of kidneys at the end point of $Trf1^{+/+}$ and $Trf1^{\Delta/\Delta}$ mice. (D) BUN levels in $Trf1^{+/+}$ and $Trf1^{\Delta/\Delta}$ mice. n=6 per group (three males; three females). No statistically significant differences were observed between sexes. (E) Analysis of urinary albumin-to-creatinine ratio (UACR). n=6 per group (three males; three females). No statistically significant differences were observed between sexes. (F) Kaplan–Meier survival curves of $Trf1^{+/+}$ and $Trf1^{\Delta/\Delta}$ mice. n=15 for $Trf1^{+/+}$ (five males; ten females) and n=24 (14 males; ten females) for $Trf1^{\Delta/\Delta}$ mice. No statistically significant differences were observed between sexes. (G) Bar graph showing distribution of pathologic lesions in organs of $Trf1^{+/+}$ and $Trf1^{\Delta/\Delta}$ mice. n=12 for $Trf1^{+/+}$ (five males; seven females) and n=23 (14 males; nine females) for $Trf1^{\Delta/\Delta}$ *mice*. No statistically significant differences were observed between sexes. (H) Representative immunofluorescence (6–8 visual fields for each tissue analyzed) stainings for Trf1 (green) and KFP (red) and quantification of the percentage of double $KFP^{+}TRF1^{+}$ fibroblasts in $Trf1^{+/+}$

Figure 6. *Continued.* and $Trf1^{\Delta/\Delta}$ kidneys. Nuclei are stained with DAPI (blue). $n=8$ for $Trf1^{+/+}$ (three males; five females) and $n=8$ for $Trf1^{\Delta/\Delta}$ (four males; four females) mice. No statistically significant differences were observed between sexes. (I–M) Representative images and quantifications (whole section analyzed) of (I) Masson trichome staining (whole section-left panel; magnified view-right panel). (J) Sirius red staining. $n=10$ for $Trf1^{+/+}$ (two males; eight females) and $n=13$ for $Trf1^{\Delta/\Delta}$ mice (eight males; five females). (K) PAS+D staining (12–15 visual fields for each tissue analyzed) and quantifications of tubular injury score. $n=6$ for $Trf1^{+/+}$ (three males; three females) and $n=6$ for $Trf1^{\Delta/\Delta}$ mice (four males; two females). (L) α-SMA. (M) F4/80 in $Trf1^{+/+}$ and $Trf1^{\Delta/\Delta}$ kidneys. $n=10$ for $Trf1^{+/+}$ (two males; eight females) and $n=13$ for $Trf1^{\Delta/\Delta}$ *mice* (eight males; five females). Animal survival was assessed by the Kaplan–Meier analysis, using the log rank (Mantel–Cox) test). Male mice are represented in green, and females are represented in pink color. Data are represented as mean±SEM. An unpaired, two-tailed Student *t* test was used.

increased α-SMA and Agt, followed by DNA damage in $Trf1^{\Delta/\Delta}$ mice, coinciding with CKD-induced cardiac fibrosis[37] (Supplemental Figure 7, C–F). Of note, the deletion of *Trf1* in renal tubular epithelial cells was maintained until the humane end point as indicated by multiplex staining with TRF1 and turbo-RFP antibodies (Figure 6H). $Trf1^{\Delta/\Delta}$ kidney displayed exacerbated tubulointerstitial injury and fibrosis accompanied by loss of brush borders, cellular vacuolization, and atrophy as well as increased α-SMA and F4/80 levels (Figure 6, I–M).

Trf1 Deletion Aggravated Folic Acid–Induced Kidney Fibrosis in Mice

To determine the contribution of TRF1 to AKI, we extended our studies to an additional model of kidney fibrosis and folic acid–induced nephropathy after short-term deletion of *Trf1*[38] (Figure 7A). No prior sample size calculation was made. We analyzed the urinary and blood parameters and found that $Trf1^{\Delta/\Delta}$ folic acid–treated mice showed increased UACR, urinary Kim-1, and Lcn2 levels (Figure 7, B and C, and Supplemental Figure 8A). The administration of folic acid is known to induce a transient elevation of BUN and blood creatinine levels at 48 hours after injection, followed by subsequent kidney dysfunction accompanied with interstitial fibrosis.[39] Consistently, folic acid–treated $Trf1^{\Delta/\Delta}$ mice showed significant increases in both BUN and creatinine levels on days 2, 7, and 14, with both BUN and creatinine levels progressively increasing after day 2, indicating kidney dysfunction as early as 48 hours after folic acid administration (Supplemental Figure 8, B and C). Folic acid–treated $Trf1^{\Delta/\Delta}$ mice exhibited increased tubulointerstitial fibrosis after 14 days compared with untreated $Trf1^{\Delta/\Delta}$, characterized by altered tubular morphology (periodic acid–Schiff with diastase), excessive myofibroblast population (α-SMA), ECM deposition (fibronectin), collagen deposition (collagen 1), and macrophage infiltration (F4/80) as compared with Folic acid–treated $Trf1^{+/+}$ and untreated $Trf1^{\Delta/\Delta}$ and $Trf1^{+/+}$ cohorts (Figure 7, D–I, and Supplemental Figure 8D).

Discussion

Renal tubulointerstitial fibrosis is one of the major pathologic features of CKD, associated with decline in kidney function.[3,40] Several studies indicate that patients with CKD and shorter leukocyte telomere length exhibit reduced kidney function associated with higher morbidity and mortality.[41–45] Mice with dysfunctional telomeres show age-dependent decline in kidney function, delayed kidney recovery, and increased fibrosis.[23,46] We have previously shown that telomerase-deficient (G3-$Tert^{-/-}$) mice had increased vulnerability of developing kidney fibrosis in response to folic acid by inducing cellular senescence and inflammation and exacerbating the EMT program.[23] Furthermore, constitutive deletion of *Trf1* in entire kidney cell population resulted in kidney fibrosis. Nevertheless, definitive contribution of *Trf1* deletion in distinct kidney cell types has remained unexplored until recently. Recently, we studied the role of renal fibroblasts in telomere dysfunction–associated fibrosis, with renal epithelial cells left completely undisturbed. However, short-term *Trf1* deletion in renal fibroblasts was insufficient to trigger kidney fibrosis but induced inflammation, ECM deposition, cell cycle arrest, fibrogenesis, and vascular rarefaction. By contrast, long-term *Trf1* deletion in fibroblasts resulted in pronounced kidney fibrosis with decline in survival and kidney function. Chronic telomere dysfunction in fibroblasts triggered macrophage-to-myofibroblast transition, endothelial-to-mesenchymal transition, and EMT, all contributing to fibrogenesis.[24]

In this study, we have for the first time explored the role of telomere dysfunction specifically in renal tubular epithelial cells. Eight weeks of *Trf1* deletion leads to severe tubule injury coincident with significant alterations in blood parameters and upregulation in Kim-1 and Lcn2, characteristic features of AKI in patients.[3] Cellular senescence in AKI is driven by the p53/p21CIP1 and p16INK4a/Rb pathways as observed in unilateral ureteral obstruction model, ischemia-reperfusion injury model, and aging kidney diseases in mouse and patients with CKD.[47–49] Telomere dysfunction activates DDR, leading to phosphorylation of histone H2AX and activation of canonical p53–p21 pathway, leading to cell cycle arrest in renal tubular epithelial cells, a crucial driver of maladaptive repair in various kidney fibrosis models.[3,50] Consistently, our results showed that *Trf1*-deficient kidneys had increased markers of cell arrest and senescence, such as p53/p21CIP1 and senescence-associated β-galactosidase expression, similarly to that described for human patients and bonafide CKD mouse models.[47–49] At the molecular level, we observed a rapid onset of persistent telomeric DNA damage (telomere induced foci) leading to cellular senescence and apoptosis.[51,52] To the best of our knowledge, this is the first study showing that telomere dysfunction specifically in renal tubular epithelial cells increases the susceptibility to develop kidney fibrosis by reducing the kidney's ability to repair itself after injury.

The activation of Ras/Raf/MEK/ERK and Ras/PI3K/phosphatase and tensin homolog/Akt/mTOR signaling pathways has previously been observed in ischemia-reperfusion, GN, diabetic rats, polycystic kidney disease, and in remnant kidneys in rats after 5/6

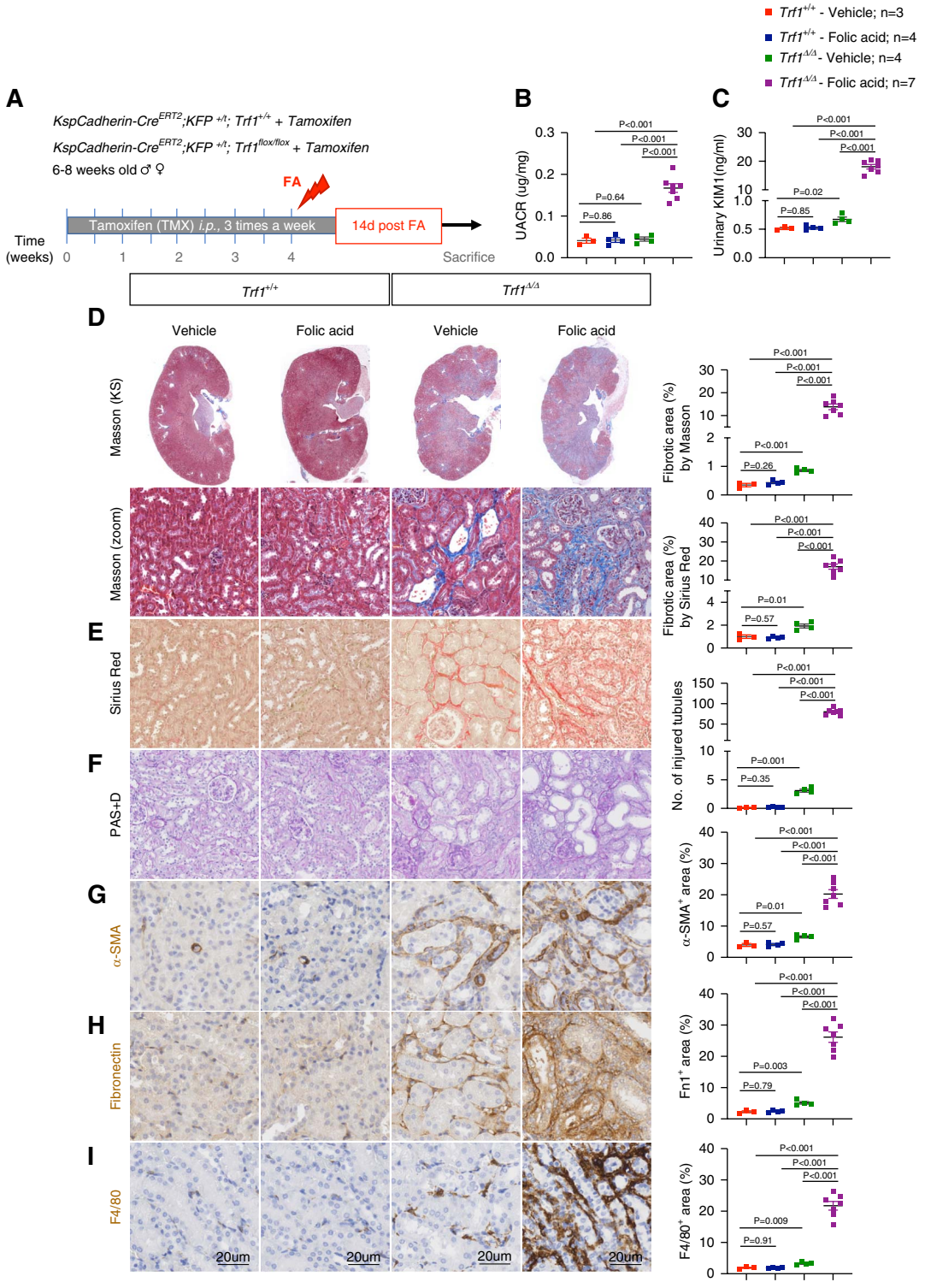

Figure 7. Renal tubular epithelial cells *Trf1* deletion exacerbates folic acid–induced mouse kidney fibrosis. (A) Schematic representation of the experimental design. (B) Analysis of UACR. (C) ELISA of urinary Kim1. (D–I) Representative images and quantifications (whole section analyzed) of (D) Masson trichome staining (whole section-top panel; magnified view-lower panel). (E) Sirius red staining. (F) PAS+D staining (12–15 visual fields for each tissue analyzed) and quantifications of tubular injury score. (G) α-SMA (whole section analyzed). (H) Fibronectin (quantifications of whole section). (I) F4/80 (whole section analyzed) in $Trf1^{+/+}$ and $Trf1^{\Delta/\Delta}$ kidneys. n=3 for $Trf1^{+/+}$—vehicle (two males; one female); n=4 for $Trf1^{+/+}$—folic acid (two males; two female); n=4 for $Trf1^{\Delta/\Delta-}$— vehicle (two males; two female); and n=7 $Trf1^{\Delta/\Delta-}$—folic acid (three males; four female). Data are represented as mean±SEM. An unpaired, two-tailed Student t test was used. FA, folic acid.

nephrectomy-induced glomerulosclerosis.[53–56] Furthermore, active phosphorylated forms of p38 Kinase are markedly increased in epithelial cells in injured kidney.[57] Consistently, $Trf1^{\Delta/\Delta}$ mice exhibited a positive correlation between upregulation of KRAS pathway and progression of kidney fibrosis. Inflammation is recognized as a pivotal contributor to kidney fibrosis primarily through the induction of proinflammatory cytokines such as TNF-α, which subsequently activate NF-κB signaling pathways.[33] The loss of *Trf1* in renal tubular epithelial cells caused increased gene expression of proinflammatory pathways and inflammatory cytokines in $Trf1^{\Delta/\Delta}$ mice. Altogether, these results indicate that TRF1 deficiency in renal tubular epithelial cells leads to increased inflammation coincidental with TNF-α signaling through NFkB and activation of the Ras/Raf/MEK/ERK and Ras/PI3K/phosphatase and tensin homolog/Akt/mTOR pathways.

Long-term TRF1 abrogation in renal tubular epithelial cells over the lifespan of mice leads to an early and significant increase in UACR, progressive collagen deposition, tubular atrophy, and tubulointerstitial injury, culminating in CKD. By contrast, long-term TRF1 depletion in fibroblasts led to much later onset of UACR elevation, increased BUN, and creatinine levels as compared with depletion in renal tubular epithelial cells, 12 versus 1.5 months post-*Trf1* deletion. Translating this timeline to human physiology, 4 months of mouse age corresponds to human age range of approximately 20–30 years, while 12 months corresponds to 38–47 years.[58–60] These findings suggest that even in young adults, loss of TRF1 in renal tubular epithelial cells could render the kidneys significantly more susceptible to fibrosis and injury compared with TRF1 loss in renal fibroblasts. This highlights the critical role of TRF1 in renal tubular epithelial cells for maintaining kidney integrity and underscores its potential as a target for preventing early-onset kidney fibrosis.

Cardiorenal syndrome is a complex pathophysiologic disorder resulting from the interplay between cardiac and kidney insufficiency.[61,62] The activation of RAAS is one of the early response systems in acute cardiorenal syndrome characterized by the presence of uAGT.[63] $Trf1^{\Delta/\Delta}$ mice displayed renal RAAS activation with upregulation of uAGT. In addition, increased collagen deposition with Agt and DNA damage in heart at humane end point was observed in TRF1-deficient mice. These observations recapitulate human disease where the incidence of chronic heart failure in patients with CKD is elevated.

It would be interesting to address the potential therapeutic efficacy of *Trf1* gene therapy or targeting telomere length as it presents a promising therapeutic avenue in CKD. Specifically, evaluating whether the restoration of *Trf1* expression or telomere length could reverse the observed fibrotic phenotype or ameliorate the progression of fibrosis would provide valuable insights into therapeutic possibilities of targeting gene therapies in the context of kidney diseases. Although our findings provide valuable mechanistic insights in animal models, translating these findings to human patients remains an essential step. Future studies could benefit from measuring *Trf1* levels and telomere shortening in kidney tissues from human patients with kidney disease. This would not only help establish the relevance of our findings in human pathology but also provide novel insights into how telomere dysfunction contributes to fibrosis in a clinical setting.

In summary, we showed that short-term *Trf1* deletion in renal tubular epithelial cells leads to kidney injury leading to an AKI that progresses to CKD at humane end point. Telomere shortening and telomeric damage, a hallmark of kidney disease and other fibrotic and aging-related conditions,[41,42] was faithfully recapitulated in our study. Our study underscores the critical importance of understanding the site of origin and specific mechanisms by which each cell type contributes to disease progression, as this knowledge is paramount for the development of targeted gene therapies. These findings pave the way to generate targeted telomere-based therapies in renal epithelial cells as a potential treatment for kidney fibrosis and CKD.

Disclosures

Disclosure forms, as provided by each author, are available with the online version of the article at http://links.lww.com/JSN/F320.

Author Contributions

Conceptualization: Maria A. Blasco.
Formal analysis: Sarita Saraswati.
Funding acquisition: Maria A. Blasco.
Investigation: Ruth Álvarez Díaz, Juana María Flores, Osvaldo Graña-Castro, Paula Martínez, Diego Mejías, Sarita Saraswati, Rosa Serrano.
Methodology: Paula Martínez, Sarita Saraswati, Rosa Serrano.
Resources: Ruth Álvarez Díaz, Osvaldo Graña-Castro, Diego Mejías.
Software: Ruth Álvarez Díaz, Osvaldo Graña-Castro, Diego Mejías, Sarita Saraswati.
Supervision: Maria A. Blasco, Paula Martínez.
Validation: Maria A. Blasco, Paula Martínez, Sarita Saraswati.
Writing – original draft: Maria A. Blasco, Sarita Saraswati.
Writing – review & editing: Maria A. Blasco, Paula Martínez, Sarita Saraswati.

Funding

M.A. Blasco: Fundación Humanismo y Ciencia, the Ministry of Science and Innovation (MCIN/AEI/10.13039/501100011033), projects SAF2017-82623-R and SAF2015-72455-EXP cofunded by the European Regional Development Fund and project CPP2021-008483, cofunded by and the European Union "NextGenerationEU"/PRTR", Comunidad de Madrid (S2017/BMD-3770), World Cancer Research Fund (16-1177), 2020 European Research Council (SHELTERINS GA882385), and Fundación Botín.

Acknowledgments

We thank the CNIO Mouse Genome Editing Unit at the CNIO for importing and establishing the Ksp-Cadherin-Cre-ER^{T2} line and providing the Tg.CAG-LSL-Katushka strain. We also thank CNIO Flow Cytometry Core Unit for technical assistance with the experimental design, cell sorting and data analysis.

Declarative Statements

All animal experiments were conducted in accordance with the NIH Guide for the Care and Use of Laboratory Animals or an

equivalent standard that meets or exceeds the ethical and welfare requirements outlined in the NIH Guide. All protocols were approved by the appropriate institutional animal care and use committee.

Data Availability Statements

Original data generated for the study are or will be made available in a public access repository upon publication. Other. Gene Expression Omnibus (GEO) Data. GEO. GSE272068. The authors declare that data supporting the findings of this study are openly available in repository GEO with IDs: GSE272068 and are available within the paper (and its supplemental material).

Supplemental Material

This article contains the following supplemental material online at http://links.lww.com/JSN/F321, http://links.lww.com/JSN/F322.

Supplemental Methods

Supplemental Figure 1. Conditional deletion of *Trf1* in renal tubular epithelial cells.

Supplemental Figure 2. Short-term *Trf1* deletion in renal tubular epithelial cells did not cause pathologies in major organs.

Supplemental Figure 3. Short-term *Trf1* deletion in renal tubular epithelial cells caused hypoxia and microvascular rarefaction.

Supplemental Figure 4. Flow cytometry cell isolation and GSEA hallmarks analysis.

Supplemental Figure 5. *Trf1* deletion in renal tubular epithelial cells prompts RAAS pathway in $Trf1^{\Delta/\Delta}$ mice.

Supplemental Figure 6. Long-term Trf1 deletion in renal tubular epithelial cells alters body weight and blood parameters in $Trf1^{\Delta/\Delta}$ mice.

Supplemental Figure 7. Effect of prolonged Trf1 deletion in renal tubular epithelial cells on major organs.

Supplemental Figure 8. Trf1 deletion in renal tubular epithelial cells exacerbates folic acid–induced mouse kidney fibrosis.

Supplemental Table 1. List of genes.

Supplemental Table 2. Reverse transcription quantitative PCR primers.

Supplemental Datasheet

References

1. Francis A, Harhay MN, Ong ACM, et al.; American Society of Nephrology, European Renal Association, International Society of Nephrology. Chronic kidney disease and the global public health agenda: an international consensus. *Nat Rev Nephrol.* 2024;20(7):473–485. doi:10.1038/s41581-024-00820-6
2. Schmitt R, Cantley LG. The impact of aging on kidney repair. *Am J Physiol Renal Physiol.* 2008;294(6):F1265–F1272. doi:10.1152/ajprenal.00543.2007
3. Ferenbach DA, Bonventre JV, Humphreys BD, et al. Mechanisms of maladaptive repair after AKI leading to accelerated kidney ageing and CKD. *Nat Rev Nephrol.* 2015;11(5):264–276. doi:10.1038/nrneph.2015.3
4. Sturmlechner I, Durik M, Sieben CJ, Baker DJ, van Deursen JM. Cellular senescence in renal ageing and disease. *Nat Rev Nephrol.* 2017;13(2):77–89. doi:10.1038/nrneph.2016.183
5. Li Z-L, Li X-Y, Zhou Y, Wang B, Lv L-L, Liu B-C. Renal tubular epithelial cells response to injury in acute kidney injury. *EBioMedicine.* 2024;107:105294. doi:10.1016/j.ebiom.2024.105294
6. Zhang J-Q, Li Y-Y, Zhang X-Y, et al. Cellular senescence of renal tubular epithelial cells in renal fibrosis. *Front Endocrinol (Lausanne).* 2023;14:1085605. doi:10.3389/fendo.2023.1085605
7. Martínez P, Blasco MA. Telomeric and extra-telomeric roles for telomerase and the telomere-binding proteins. *Nat Rev Cancer.* 2011;11(3):161–176. doi:10.1038/nrc3025
8. Martínez P, Blasco MA. Role of shelterin in cancer and aging. *Aging Cell.* 2010;9(5):653–666. doi:10.1111/j.1474-9726.2010.00596.x
9. Palm W, de Lange T. How shelterin protects mammalian telomeres. *Annu Rev Genet.* 2008;42:301–334. doi:10.1146/annurev.genet.41.110306.130350
10. Harley CB, Futcher AB, Greider CW. Telomeres shorten during ageing of human fibroblasts. *Nature.* 1990;345(6274):458–460. doi:10.1038/345458a0
11. Shore D, Bianchi A. Telomere length regulation: coupling DNA end processing to feedback regulation of telomerase. *EMBO J.* 2009;28(16):2309–2322. doi:10.1038/emboj.2009.195
12. Martínez P, Thanasoula M, Muñoz P, et al. Increased telomere fragility and fusions resulting from TRF1 deficiency lead to degenerative pathologies and increased cancer in mice. *Genes Dev.* 2009;23(17):2060–2075. doi:10.1101/gad.543509
13. Sfeir A, Kosiyatrakul ST, Hockemeyer D, et al. Mammalian telomeres resemble fragile sites and require TRF1 for efficient replication. *Cell.* 2009;138(1):90–103. doi:10.1016/j.cell.2009.06.021
14. Povedano JM, Martinez P, Serrano R, et al. Therapeutic effects of telomerase in mice with pulmonary fibrosis induced by damage to the lungs and short telomeres. *eLife.* 2018;7:e31299. doi:10.7554/eLife.31299
15. Povedano JM, Martinez P, Flores JM, Mulero F, Blasco MA. Mice with pulmonary fibrosis driven by telomere dysfunction. *Cell Rep.* 2015;12(2):286–299. doi:10.1016/j.celrep.2015.06.028
16. Piñeiro-Hermida S, Martínez P, Bosso G, et al. Consequences of telomere dysfunction in fibroblasts, club and basal cells for lung fibrosis development. *Nat Commun.* 2022;13(1):5656. doi:10.1038/s41467-022-32771-6
17. Beier F, Foronda M, Martinez P, Blasco MA. Conditional TRF1 knockout in the hematopoietic compartment leads to bone marrow failure and recapitulates clinical features of dyskeratosis congenita. *Blood.* 2012;120(15):2990–3000. doi:10.1182/blood-2012-03-418038
18. Westhoff JH, Schildhorn C, Jacobi C, et al. Telomere shortening reduces regenerative capacity after acute kidney injury. *J Am Soc Nephrol.* 2010;21(2):327–336. doi:10.1681/ASN.2009010072
19. Cheng H, Fan X, Lawson WE, Paueksakon P, Harris RC. Telomerase deficiency delays renal recovery in mice after ischemia–reperfusion injury by impairing autophagy. *Kidney Int.* 2015;88(1):85–94. doi:10.1038/ki.2015.69
20. Quimby JM, Maranon DG, Battaglia CLR, McLeland SM, Brock WT, Bailey SM. Feline chronic kidney disease is associated with shortened telomeres and increased cellular senescence. *Am J Physiol Renal Physiol.* 2013;305(3):F295–F303. doi:10.1152/ajprenal.00527.2012
21. Park S, Lee S, Kim Y, et al. A Mendelian randomization study found causal linkage between telomere attrition and chronic kidney disease. *Kidney Int.* 2021;100(5):1063–1070. doi:10.1016/j.kint.2021.06.041
22. Fazzini F, Lamina C, Raschenberger J, et al.; GCKD Investigators. Results from the German Chronic Kidney Disease (GCKD) study support association of relative telomere length with mortality in a large cohort of patients with moderate chronic kidney disease. *Kidney Int.* 2020;98(2):488–497. doi:10.1016/j.kint.2020.02.034
23. Saraswati S, Martínez P, Graña-Castro O, Blasco MA. Short and dysfunctional telomeres sensitize the kidneys to develop fibrosis. *Nat Aging.* 2021;1(3):269–283. doi:10.1038/s43587-021-00040-8
24. Saraswati S, Martínez P, Serrano R, et al. Renal fibroblasts are involved in fibrogenic changes in kidney fibrosis associated with dysfunctional telomeres. *Exp Mol Med.* 2024;56(10):2216–2230. doi:10.1038/s12276-024-01318-8
25. Whyte DA, Li C, Thomson RB, et al. Ksp-cadherin gene promoter. I. Characterization and renal epithelial cell-specific activity. *Am J Physiol.* 1999;277(4):F587–F598. doi:10.1152/ajprenal.1999.277.4.F587
26. Igarashi P, Shashikant CS, Thomson RB, et al. Ksp-cadherin gene promoter. II. Kidney-specific activity in transgenic mice. *Am J Physiol.* 1999;277(4):F599–F610. doi:10.1152/ajprenal.1999.277.4.F599

27. Diéguez-Hurtado R, Martín J, Martínez-Corral I, et al. A Cre-reporter transgenic mouse expressing the far-red fluorescent protein Katushka. *Genesis.* 2011;49(1):36–45. doi:10.1002/dvg.20685
28. Djudjaj S, Papasotiriou M, Bülow RD, et al. Keratins are novel markers of renal epithelial cell injury. *Kidney Int.* 2016;89(4):792–808. doi:10.1016/j.kint.2015.10.015
29. Kumar S, Liu J, Pang P, et al. Sox9 activation highlights a cellular pathway of renal repair in the acutely injured mammalian kidney. *Cell Rep.* 2015;12(8):1325–1338. doi:10.1016/j.celrep.2015.07.034
30. Prommer H-U, Maurer J, von Websky K, et al. Chronic kidney disease induces a systemic microangiopathy, tissue hypoxia and dysfunctional angiogenesis. *Sci Rep.* 2018;8(1):5317. doi:10.1038/s41598-018-23663-1
31. Rouillard AD, Gundersen GW, Fernandez NF, et al. The harmonizome: a collection of processed datasets gathered to serve and mine knowledge about genes and proteins. *Database (Oxford).* 2016;2016:baw100. doi:10.1093/database/baw100
32. Pak C, Miyamoto S. A new alpha in line between KRAS and NF-κB activation? *Cancer Discov.* 2013;3(6):613–615. doi:10.1158/2159-8290.CD-13-0193
33. Zoccali C, Vanholder R, Massy ZA, et al.; European Renal and Cardiovascular Medicine (EURECA-m) Working Group of the European Renal Association – European Dialysis Transplantation Association (ERA-EDTA). The systemic nature of CKD. *Nat Rev Nephrol.* 2017;13(6):344–358. doi:10.1038/nrneph.2017.52
34. Ma K, Gao W, Xu H, Liang W, Ma G. Role and mechanism of the renin-angiotensin-aldosterone system in the onset and development of cardiorenal syndrome. *J Renin Angiotensin Aldosterone Syst.* 2022;2022:3239057. doi:10.1155/2022/3239057
35. Jin H-Y, Chen L-J, Zhang Z-Z, et al. Deletion of angiotensin-converting enzyme 2 exacerbates renal inflammation and injury in apolipoprotein E-deficient mice through modulation of the nephrin and TNF-alpha-TNFRSF1A signaling. *J Transl Med.* 2015;13:255. doi:10.1186/s12967-015-0616-8
36. Zhang X, Ding X, Lv W-L, Teng J, Zhong Y-H. ELISA examining urinary angiotensinogen as a potential indicator of intrarenal renin-angiotensin system (RAS) activity: a clinical study of 128 chronic kidney disease patients. *Mol Biol Rep.* 2013;40(10):5817–5824. doi:10.1007/s11033-013-2687-z
37. Romero-González G, González A, López B, Ravassa S, Díez J. Heart failure in chronic kidney disease: the emerging role of myocardial fibrosis. *Nephrol Dial Transplant.* 2022;37(5):817–824. doi:10.1093/ndt/gfaa284
38. Yang H-C, Zuo Y, Fogo AB. Models of chronic kidney disease. *Drug Discov Today Dis Models.* 2010;7(1-2):13–19. doi:10.1016/j.ddmod.2010.08.002
39. Long DA, Woolf AS, Suda T, Yuan HT. Increased renal angiopoietin-1 expression in folic acid-induced nephrotoxicity in mice. *J Am Soc Nephrol.* 2001;12(12):2721–2731. doi:10.1681/ASN.V12122721
40. Liu B-C, Tang T-T, Lv L-L, Lan H-Y. Renal tubule injury: a driving force toward chronic kidney disease. *Kidney Int.* 2018;93(3):568–579. doi:10.1016/j.kint.2017.09.033
41. Akinnibosun OA, Maier MC, Eales J, Tomaszewski M, Charchar FJ. Telomere therapy for chronic kidney disease. *Epigenomics.* 2022;14(17):1039–1054. doi:10.2217/epi-2022-0073
42. Levstek T, Trebušak Podkrajšek K. Telomere attrition in chronic kidney diseases. *Antioxidants (Basel).* 2023;12(3):579. doi:10.3390/antiox12030579
43. Betjes MGH, Langerak AW, van der Spek A, de Wit EA, Litjens NHR. Litjens NHR: premature aging of circulating T cells in patients with end-stage renal disease. *Kidney Int.* 2011;80(2):208–217. doi:10.1038/ki.2011.110
44. Kato S, Shiels PG, McGuinness D, et al. Telomere attrition and elongation after chronic dialysis initiation in patients with end-stage renal disease. *Blood Purif.* 2016;41(1-3):25–33. doi:10.1159/000440971
45. Gurung RL, M Y, Liu S, Liu J-J, Lim SC. Short leukocyte telomere length predicts albuminuria progression in individuals with type 2 diabetes. *Kidney Int Rep.* 2018;3(3):592–601. doi:10.1016/j.ekir.2017.12.005
46. Schildhorn C, Jacobi C, Weissbrodt A, et al. Renal phenotype of young and old telomerase-deficient mice. *Mech Ageing Dev.* 2015;150:65–73. doi:10.1016/j.mad.2015.08.004
47. Docherty M-H, O'Sullivan ED, Bonventre JV, Ferenbach DA. Cellular senescence in the kidney. *J Am Soc Nephrol.* 2019;30(5):726–736. doi:10.1681/ASN.2018121251
48. Mylonas KJ, O'Sullivan ED, Humphries D, et al. Cellular senescence inhibits renal regeneration after injury in mice, with senolytic treatment promoting repair. *Sci Transl Med.* 2021;13(594):eabb0203. doi:10.1126/scitranslmed.abb0203
49. Rex N, Melk A, Schmitt R. Cellular senescence and kidney aging. *Clin Sci (Lond).* 2023;137(24):1805–1821. doi:10.1042/CS20230140
50. Huang W, Hickson LJ, Eirin A, Kirkland JL, Lerman LO. Cellular senescence: the good, the bad and the unknown. *Nat Rev Nephrol.* 2022;18(10):611–627. doi:10.1038/s41581-022-00601-z
51. Smogorzewska A, de Lange T. Different telomere damage signaling pathways in human and mouse cells. *EMBO J.* 2002;21(16):4338–4348. doi:10.1093/emboj/cdf433
52. Martínez P, Blasco MA. Telomere-driven diseases and telomere-targeting therapies. *J Cell Biol.* 2017;216(4):875–887. doi:10.1083/jcb.201610111
53. Muñoz-Félix JM, Martínez-Salgado C. Dissecting the involvement of Ras GTPases in kidney fibrosis. *Genes (Basel).* 2021;12(6):800. doi:10.3390/genes12060800
54. Kwon DS, Kwon CH, Kim JH, Woo JS, Jung JS, Kim YK. Signal transduction of MEK/ERK and PI3K/Akt activation by hypoxia/reoxygenation in renal epithelial cells. *Eur J Cell Biol.* 2006;85(11):1189–1199. doi:10.1016/j.ejcb.2006.06.001
55. Gui Y, Dai C. mTOR signaling in kidney diseases. *Kidney360.* 2020;1(11):1319–1327. doi:10.34067/KID.0003782020
56. Wang H, Gao L, Zhao C, et al. The role of PI3K/Akt signaling pathway in chronic kidney disease. *Int Urol Nephrol.* 2024;56(8):2623–2633. doi:10.1007/s11255-024-03989-8
57. Ma FY, Tesch GH, Nikolic-Paterson DJ. ASK1/p38 signaling in renal tubular epithelial cells promotes renal fibrosis in the mouse obstructed kidney. *Am J Physiol Renal Physiol.* 2014;307(11):F1263–F1273. doi:10.1152/ajprenal.00211.2014
58. Dutta S, Sengupta P. Men and mice: relating their ages. *Life Sci.* 2016;152:244–248. doi:10.1016/j.lfs.2015.10.025
59. Wang S, Lai X, Deng Y, Song Y. Correlation between mouse age and human age in anti-tumor research: significance and method establishment. *Life Sci.* 2020;242:117242. doi:10.1016/j.lfs.2019.117242
60. Flurkey K, Currer J M, Harrison DE. Chapter 20 - mouse models in aging research [internet]. In: Fox JG, Davisson MT, Quimby FW, Barthold SW, Newcomer CE, Smith AL, eds. *The Mouse in Biomedical Research (Second Edition)*; 2007:637–672.
61. Melenovsky V, Cervenka L, Viklicky O, et al. Kidney response to heart failure: proteomic analysis of cardiorenal syndrome. *Kidney Blood Press Res.* 2018;43(5):1437–1450. doi:10.1159/000493657
62. Kumar U, Wettersten N, Garimella PS. Cardiorenal syndrome: pathophysiology. *Cardiol Clin.* 2019;37(3):251–265. doi:10.1016/j.ccl.2019.04.001
63. Kahlon T, Carlisle S, Otero Mostacero D, Williams N, Trainor P, DeFilippis AP. Angiotensinogen: more than its downstream products: evidence from population studies and novel therapeutics. *JACC Heart Fail.* 2022;10(10):699–713. doi:10.1016/j.jchf.2022.06.005